AIMS Energy
https://www.aimspress.com/journal/energy

AIMS Energy, 13(6): 1583–1608.
DOI: 10.3934/energy.2025059
Received: 11 August 2025
Revised: 06 December 2025
Accepted: 11 December 2025
Published: 18 December 2025

Research article

Improved modeling of real photovoltaic panel efficiency using a fractional-order error function family

Leonardo Martínez–Jiménez[1], **Jorge Manuel Barrios–Sánchez**[1,2*], **Roberto Baeza–Serrato**[1]

[1] Department of Multidisciplinary Studies, DICIS, University of Guanajuato, Yuriria, Gto 38940, México

[2] Corporación Universitaria Rafael Núñez, Colombia

* **Correspondence:** Email: jorge.barrios@campusuninunez.edu.co; Tel: +573107196449.

Abstract: In this study, we introduced a unified family of fractional-order derivatives of the error function, bridging classical error function ($\alpha = 0$) and Gaussian ($\alpha = 1$) through Maclaurin expansion and Lacroix's fractional calculus. The adaptive model was validated against cubic spline and Gaussian baselines using six days of real photovoltaic measurements from a tropical environment. Moving-window optimization achieved competitive accuracy (Root Mean Squared Error (RMSE): 0.0083–0.0104; Mean Absolute Error (MAE) 0.0068–0.0086) while preserving physical interpretability via the fractional order α. Comparative analysis demonstrated significant improvement over Gaussian fitting, with an average 14.17% reduction in RMSE across all test days. The fractional approach also delivered more consistent daily performance and better captured asymmetric transitions, despite spline's occasional marginal RMSE advantages. Graphical analysis revealed persistent diurnal α patterns: from 0.50 at sunrise, peaking at 0.90–0.91 near noon, declining to 0.37 afternoon, with sunset rebound. Our results confirmed the model effectively captures photovoltaic memory effects while offering superior interpretability and dynamic adaptation versus traditional methods. The framework enables accurate energy forecasting and condition-based maintenance, with future work focusing on real-time α tuning and machine learning integration.

Keywords: fractional calculus; error function; photovoltaic efficiency modeling; adaptive optimization; memory effects; solar energy; diurnal dynamics

---

Nomenclature: t: time in hours (0–24); x: normalized time variable, $x = (t - \text{mid\_point})/\text{spread}$; α: adaptive fractional order estimated for each window; $\Phi_\alpha(x)$: proposed fractional-order error function; $\Phi(x)$: classical error function ($\alpha = 0$); $\phi(x)$: Gaussian function, derivative of $\Phi(x)$ ($\alpha = 1$) ; n: summation index in the Maclaurin expansion; N: total number of sliding windows; w: window index; window size: number of data points in each window; $E(t)$: measured photovoltaic efficiency; $\hat{E}(t)$: modeled efficiency using the fractional approach; $\hat{E}_{\text{spline}}(t)$: modeled efficiency using cubic spline;

$\hat{E}_{\text{gauss}}(t)$: modeled efficiency using Gaussian fit; $\Gamma(\cdot)$: Euler Gamma function; RMSE: Root Mean Squared Error; MAE: Mean Absolute Error; p: smoothing parameter for cubic spline (if applied); A, μ, σ, b: Gaussian model parameters (amplitude, mean, width, baseline)

1. Introduction

The global energy landscape is undergoing a profound transformation, driven by a growing awareness of climate change and the urgent need to transition toward sustainable energy sources. In this context, photovoltaic (PV) systems have solidified their position as a cornerstone of clean electricity generation, offering a promising solution to meet global energy demand and mitigate greenhouse gas emissions. The efficiency with which these panels convert sunlight into electricity is a critical parameter determining their economic viability, effective grid integration, and genuine contribution to sustainability goals [1]. Therefore, accurate modeling of PV panel efficiency is of paramount importance for their optimal design, performance prediction, and long-term strategic planning.

However, the actual efficiency of photovoltaic panels under operational conditions is an inherently complex and dynamic phenomenon, influenced by a multitude of environmental and operational factors. Elements such as fluctuating solar irradiance, significant variations in ambient temperature [2, 3], dust and dirt accumulation on the panel surface [4–6], and challenges associated with thermal management [7–9] contribute to non-linear behavior and the manifestation of memory effects or historical dependencies in the panel's performance. These phenomena, where the current state of the system depends not only on immediate conditions but also on its past history, pose significant challenges for accurate modeling using conventional integer-order derivative approaches.

While modeling strategies have been explored in recent years—including data-driven and learning-based frameworks [10–12] traditional approaches such as cubic spline interpolation and Gaussian fitting remain widely used for photovoltaic performance analysis. However, these methods present limitations: Spline interpolation lacks physical interpretability despite exact data fitting, while Gaussian fitting struggles to capture asymmetric daily patterns and memory effects inherent in real PV systems. Here, we addresses these limitations through a novel fractional-order error function approach that provides both mathematical rigor and physical interpretability, with comprehensive validation against established baseline methods.

Unlike fractional-calculus applications in photovoltaic modeling that primarily employ fixed-order operators, we introduce a continuously adaptive fractional-order error function that dynamically interpolates between classical error function ($\alpha = 0$) and Gaussian ($\alpha = 1$) behavior. Key innovations include real-time optimization of the fractional order α through moving windows, direct physical interpretation of α as a memory indicator, and rigorous statistical validation against baseline models using experimental data from tropical conditions.

The error function, a transcendental function defined through the integral of the normal distribution, emerges as a fundamental element in various branches of mathematics, particularly in the solutions of differential equations and in probability theory. In the realm of physics, it is frequently associated with the description of diffusion problems and Brownian motion [13], nonlinear phase modulation systems [14], and in the study of the psychometric function [15, 16]. Its mathematical properties make it suitable for describing a wide range of physical phenomena that exhibit a gradual distribution or a transition.

On the other hand, Fractional Calculus (FC) represents a mathematical discipline dedicated to the study of operators—derivatives and integrals—of arbitrary (i.e., non-integer) order. Its origins trace back to Leibniz's classic question about extending the notion of differentiation to fractional orders. Although the field initially evolved as a theoretical branch of mathematics, the development of precise measurement technologies revealed that classical integer-order models often failed to capture the memory and non-local phenomena observed in real physical systems. This gap motivated the search for more general frameworks.

Early foundational contributions, such as those by Oldham and Spanier [17], and later by Miller and Ross [18], established the basic theoretical structure of FC. Podlubny's seminal monograph [19] further consolidated the analytical and numerical tools needed for solving fractional differential equations, thereby broadening the applicability of the field.

Subsequent works expanded FC toward modern modeling and engineering practice. Baleanu and collaborators [20, 22] advanced the use of fractional operators in control, nanotechnology, and applied physics, while Golmankhaneh and Lambert [21] contributed to the understanding of fractional dynamical systems. Uchaikin's text [23] provided a comprehensive treatment of fractional derivatives for physicists and engineers, strengthening the link between FC and complex physical processes.

Furthermore, key mathematical developments—such as Wyss's formulation of the fractional diffusion equation [24] and Westerlund's work on causality in systems with memory [25] demonstrated the relevance of fractional operators for describing anomalous transport, hereditary behavior, and long-range temporal dependence.

Collectively, these contributions laid the theoretical and applied foundations that motivate the present study, emphasizing the suitability of fractional-order formulations for modeling systems governed by memory effects, such as photovoltaic energy conversion.

Definitions of fractional derivatives coexist, each with specific characteristics and applications. The Riemann-Liouville (RL) definition is one of the most classical and comprehensive; however, its fractional-order initial conditions often lack direct physical meaning, making it less convenient for formulating real problems. In contrast, the Caputo fractional derivative is distinguished by employing initial conditions given by integer-order derivatives, which provides it with direct physical meaning and facilitates its application in practical problems [26]. Nevertheless, RL and Caputo definitions utilize a singular kernel, which may limit their ability to accurately describe the full memory effect in certain systems. To overcome this limitation, more definitions with regular kernels have emerged, such as the one proposed in [27], the Atangana-Baleanu fractional derivative, which uses the Mittag-Leffler function as its kernel [28], and the conformable fractional derivative [29]. A historical milestone in the development of FC was the proposal of the Grünwald-Letnikov fractional derivative (GLFD) in 1867, based on finite differences and equivalent to the RL definition [30].

The first documented physical application of FC is attributed to Abel in 1819, who used it to solve an integral related to the tautochrone curve [31]. Since then, FC has demonstrated its versatility and effectiveness in a multitude of areas of science and engineering. Its applications range from image processing, in tasks such as edge detection [32, 33], to obtaining solutions for the Schrödinger equation using the conformable derivative [34]. In the field of energy systems, it has been employed for the analysis of installed photovoltaic capacity in Mexico using conformable derivatives [35], and for analyzing efficiency behavior in balancing loops within system dynamics environments [36], reinforcing its direct relevance to solar energy studies. Furthermore, it has found application in describing the electrical properties of metals [37], the analysis of electrical circuits [38], and in the design and control of systems with fractional stability [39]. FC has been successfully applied in advanced system identification and control, such as the design of auxiliary model-based normalized fractional gradient algorithms for nonlinear output-error systems [40] and fractional hierarchical gradient descent algorithms for parameter estimation of nonlinear control autoregressive systems [41]. In biomedical engineering, novel nonlinear fractional-order models have been developed for Parkinson's disease, analyzing brain electrical activity rhythms through intelligent adaptive Bayesian networks [42], and designing fractional innate immune responses with therapeutic interventions using intelligent machine predictive exogenous networks [43].

In this context of seeking more precise models for complex and dynamic systems such as photovoltaic panels, and recognizing the profound potential of fractional calculus to describe phenomena exhibiting memory and historical dependencies qualities highly relevant to the behavior of PV panels under varying and time-dependent conditions we propose a novel application of the family of curves based on the fractional-order error function. This innovative mathematical tool is utilized to model the efficiency of photovoltaic panels. To validate the effectiveness of the proposed approach, the methodology is rigorously applied and evaluated using real efficiency data collected over six consecutive days from operational photovoltaic panels at a private university in Cartagena de Indias, Colombia. This location (Latitude: 10.4295° N, Longitude: –75.5380° W, approximate altitude: 2 meters above sea level) is characterized by climatic conditions typical of the humid tropics, with an average daily temperature between 26 °C and 38 °C, a very favorable average solar irradiance (around 5.2 to 5.8 kWh/m²/day), and a relative humidity frequently above 80%. These operating conditions, marked by high solar radiation throughout the year but also by the presence of clouds, sea breeze, and significant transient temperature changes, are ideal for justifying the necessity of a model capable of capturing complex dynamics and inherent memory effects.

Based on this framework, the key contributions of this study are as follows:

- Novel mathematical framework: Development of a unified family of fractional-order error functions that continuously interpolate between the classical error function ($\alpha = 0$) and its Gaussian derivative ($\alpha = 1$), grounded in Lacroix's fractional derivative and the Maclaurin series expansion.
- Adaptive modeling of photovoltaic efficiency: Implementation of a sliding-window local optimization scheme for the fractional order α, capable of capturing non-stationary variations in daily photovoltaic panel efficiency.
- Experimental validation in tropical environment: Rigorous application of the model to real photovoltaic efficiency data measured over six consecutive days in Cartagena de Indias, Colombia, under high-irradiance, high-humidity, and transient thermal variation conditions.
- Comparative analysis with baseline models: Comprehensive statistical validation against cubic spline interpolation and Gaussian fitting, demonstrating advantages in physical interpretability and adaptation to asymmetric patterns.
- Analysis of α dynamics: Examination of daily evolution patterns of the fractional order and their relationship to irradiance and temperature conditions, revealing recovery of integer-order dynamics at radiation peaks.

- Potential for real-time implementation: Discussion of feasibility for integrating the model into adaptive control systems and intelligent energy performance prediction frameworks, with applications in generation forecasting and early anomaly detection.

2. Mathematical foundations

Before implementing the proposed modeling methodology, it is essential to establish the mathematical foundations that support this work. In this section, we provide the necessary background for understanding the construction of a new family of curves based on the fractional-order derivative of the error function. First, we present the classical formulation of the error function and its Maclaurin series expansion. Then, we introduce the concept of fractional derivatives, using the fractional derivative proposed by Lacroix, which facilitates analytical development and is the core of the fractional error function used in this study.

2.1. *The error function*

The error function is defined by

$$erf(x) = \frac{2}{\sqrt{\pi}} \int_0^x e^{-t^2} dt, \tag{2.1}$$

and its representation on Maclaurin's series is given by

$$erf(x) = \frac{2}{\sqrt{\pi}} \sum_{n=0}^{\infty} \frac{(-1)^n \, x^{2n+1}}{n! \, (2n+1)} = \frac{2}{\sqrt{\pi}} \left[x - \frac{x^3}{3} + \frac{x^5}{10} - \frac{x^7}{42} + \cdots \right]. \tag{2.2}$$

2.2. *Lacroix's fractional derivative*

In 1819, Sylvestre François Lacroix presented a development to express the fractional derivative of the function $y = x^m$, all as a simple mathematical exercise [44, 45]. Despite being a very simple result, it has had far-reaching implications.

Calculating the n-order derivative of the function $y = x^m$, gives

$$\frac{d^n y}{dx^n} = \frac{m!}{(m-n)!} x^{m-n}, \quad m \leq n \tag{2.3}$$

where $m, n \in \mathbb{Z}_+$.

The derivative of order α, where $\alpha \in \mathbb{R}$ is built using the properties of the gamma function $\Gamma(\cdot)$

$$\frac{d^\alpha y}{dx^\alpha} = D_x^\alpha y = \frac{\Gamma(m+1)}{\Gamma(m-\alpha+1)} x^{m-\alpha} \tag{2.4}$$

$\alpha \in \mathbb{R}$ and $\alpha \in [0, \infty)$.

3. Theoretical development and analysis

To ensure the mathematical soundness of the proposed fractional-order error function and to understand its fundamental properties, we present a detailed theoretical development. The construction of the function is based on a fractional generalization of the classical error function, where the derivative order is allowed to vary continuously between zero and one. This generalized form allows us to interpolate between the error function itself and its first derivative, which corresponds to the Gaussian function.

In the first part of this section, we address the convergence of the resulting series expression. By applying the d'Alembert ratio test, we verify that the fractional-order formulation converges absolutely for all real values of the independent variable x, a necessary condition for the stability and usability of the model in practical applications.

Following the convergence analysis, two special cases are examined: When $\alpha = 0$ and $\alpha = 1$. These values demonstrate that the proposed series formulation consistently recovers the classical error function and its Gaussian derivative, respectively, thereby validating the correctness of the generalized model at both ends of the fractional spectrum.

Finally, we explore the qualitative behavior of the function across different values of the fractional order α, by plotting its shape over a fixed domain of x. This graphical analysis provides insight into how the fractional order influences the curve's characteristics, which is essential for understanding its role in the modeling of photovoltaic efficiency in later sections. Overall, this theoretical foundation ensures that the mathematical object introduced is internally consistent and suitable for the adaptive modeling framework developed in this study.

3.1. Development of the fractional error function

Applying the Lacroix fractional derivative on the expanded error function (2.2) yields.

$$D_x^{\alpha}\left[erf(x)\right] = \frac{d^{\alpha}}{dx^{\alpha}}\left[\frac{2}{\sqrt{\pi}}\sum_{n=0}^{\infty}\frac{(-1)^n\, x^{2n+1}}{n!\,(2n+1)}\right], \tag{3.1}$$

and simplifying the α-derived series gives

$$D_x^{\alpha}\left[erf(x)\right] = \frac{2}{\sqrt{\pi}}\sum_{n=0}^{\infty}\frac{(-1)^n\,(2n)!\, x^{2n+1-\alpha}}{n!\,\Gamma\left[2(n+1)-\alpha\right]}. \tag{3.2}$$

These expressions provide a generalized form of the error function through a fractional-order derivative framework, that can capture intermediate behaviors between the classical error function and its Gaussian derivative. The resulting family of curves varies smoothly with the order parameter α, offering a flexible mathematical tool for modeling phenomena where memory effects or smooth transitions are present. In the context of this study, this formulation is particularly suitable for describing the non-instantaneous and history-dependent efficiency behavior of photovoltaic panels under real operating conditions. In the following sections will demonstrate how this theoretical construct is applied to real data and how the fractional order α can be optimized adaptively to better fit the dynamic characteristics of PV efficiency.

This new fractional order function $D_x^{\alpha}\left[\mathrm{erf}(x)\right]$ smoothly interpolates between $\mathrm{erf}(x)$ and its first derivative, the Gaussian function, as α varies from 0 to 1. In order to prove that the new expression is able to capture the smooth transition between the error function and the Gaussian function, we analyze its mathematical properties and validate it through numerical simulations.

Convergence: To test the convergence of the series, the probe's Alembert is applied to the resulting series. Let

$$a_n(\alpha) = \frac{2}{\sqrt{\pi}} \frac{(-1)^n \, (2n)!}{n! \, \Gamma(2n + 2 - \alpha)} x^{2n+1-\alpha}, \tag{3.3}$$

and applying the limit

$$\lim_{n\to\infty} \left| \frac{a_{n+1}}{a_n} \right| = \lim_{n\to\infty} \left| \frac{\frac{(-1)^{n+1} \, \Gamma(2(n+1)+1)}{(n+1)! \, \Gamma(2(n+1)+2-\alpha)}}{\frac{(-1)^n \, \Gamma(2n+1)}{n! \, \Gamma(2n+2-\alpha)}} \right|, \tag{3.4}$$

simplifies

$$\lim_{n\to\infty} \left| \frac{(2n+2)(2n+1)}{(n+1)(2n-\alpha+4)(2n-\alpha+3)} x^2 \right| \to s(\alpha)x^2, \tag{3.5}$$

where $s(\alpha)$ is an expression depending on α, since

$$\lim_{n\to\infty} \left| \frac{a_{n+1}}{a_n} \right| < 1. \tag{3.6}$$

The series converges absolutely. Furthermore, if $s(\alpha) \, x^2 \to 0$, when $x \to 0$, and x is finite for all $x \in \mathbb{R}$, the series converges for all $x \in \mathbb{R}$.

The limit obtained in Eq (3.5) follows from the asymptotic behavior of ratios of Gamma functions, which admit a well-defined expansion for large n. In particular, the convergence expressed through $s(\alpha)x^2$ is consistent with the general results presented by Paris [46], where the asymptotics of Γ-ratio structures are rigorously analyzed. This ensures that the application of the d'Alembert criterion to the term in Eq (3.3) is mathematically justified and that the resulting series is absolutely convergent for all $x \in \mathbb{R}$. Furthermore, the fractional formulation used in this work aligns with modern fractional-calculus frameworks employing nonlocal operators with weakly singular kernels [28], and the series-based construction is consistent with the analytic expansion properties discussed in [47]. Finally, the special cases $\alpha = 0$ and $\alpha = 1$ recover the classical error function and its Gaussian derivative, respectively, consistent with the standard properties reported in [48].

Special cases: The formulation recovers the classical limits:

- The case when $\alpha = 0$:

$$D_x^{\alpha} \left[erf(x) \right]_{\alpha=0} = \frac{2}{\sqrt{\pi}} \sum_{n=0}^{\infty} \frac{(-1)^n \, (2n)! \, x^{2n+1}}{n! \, \Gamma\left[2(n+1)\right]}, \tag{3.7}$$

simplifying with the properties of the gamma function: $\Gamma(n + 1) = n!$, if $n \in \mathbb{Z}_+$.

$$D_x^{\alpha} \left[erf(x) \right]_{\alpha=0} = \frac{2}{\sqrt{\pi}} \sum_{n=0}^{\infty} \frac{(-1)^n \; x^{2n+1}}{n! \; (2n+1)} = erf(x). \tag{3.8}$$

If $\alpha = 0$, the fractional expression returns to the traditional error function $erf(x)$, (2.2).

- The case when $\alpha = 1$:

$$D_x^{\alpha} \left[erf(x) \right]_{\alpha=1} = \frac{2}{\sqrt{\pi}} \sum_{n=0}^{\infty} \frac{(-1)^n \, (2n)! \, x^{2n+1-1}}{n! \, \Gamma\left[2(n+1)-1\right]}, \tag{3.9}$$

reducing, and using the property $\Gamma(2n+1) = (2n)!$

$$D_x^{\alpha}\left[erf(x)\right]_{\alpha=1} = \frac{2}{\sqrt{\pi}} \sum_{n=0}^{\infty} \frac{(-1)^n\,(2n)!\;x^{2n}}{n!\;(2n)!}, \tag{3.10}$$

simplifying

$$D_x^{\alpha}\left[erf(x)\right]_{\alpha=1} = \frac{2}{\sqrt{\pi}} \sum_{n=0}^{\infty} \frac{(-1)^n\;\;x^{2n}}{n!} = \frac{2}{\sqrt{\pi}}e^{-x^2} \tag{3.11}$$

It is shown that, by using the fractional order $\alpha = 1$ in the Eq (3.2), the result coincides with the first derivative of the error function, which is the Gaussian function.

Behavior with varying α: The function was evaluated for $0 \le \alpha \le 1$ and $0 \le x \le 3$. Figure 1 illustrates the continuous transition from $erf(x)$ ($\alpha = 0$) to the Gaussian ($\alpha = 1$); only the real part is plotted when complex values arise for certain parameter combinations.

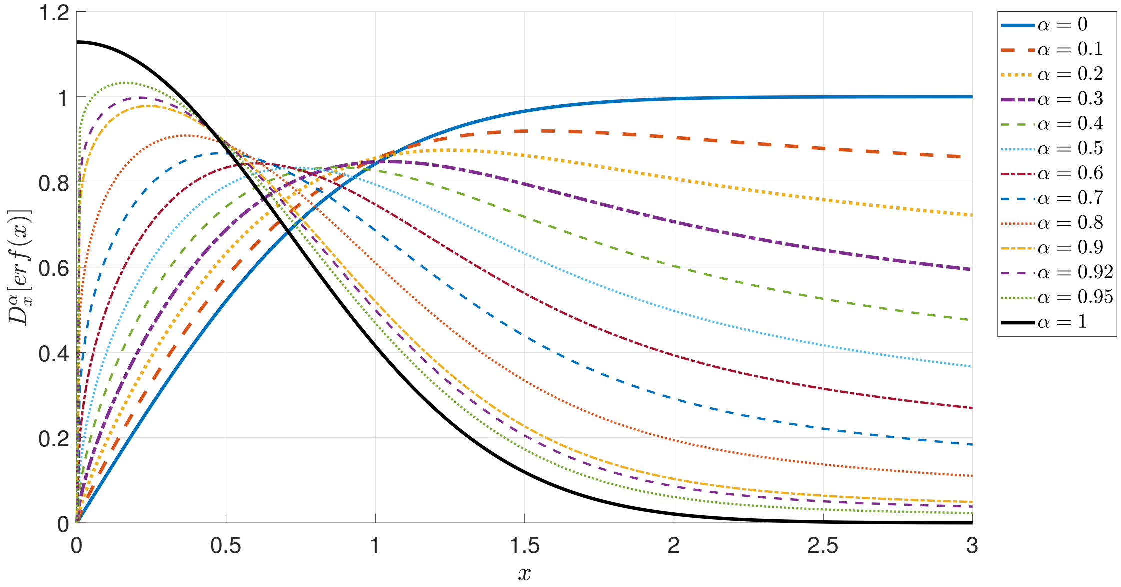

Figure 1. Fractional error function for representative values of α.

Figure 1 reveals the full behavioral spectrum of the fractional error function $D_x^{\alpha}[\mathrm{erf}(x)]$ as order α varies from 0 to 1. For $\alpha = 0$, the curve corresponds to the classical error function, exhibiting its characteristic sigmoid shape and monotonic growth toward unity. As soon as α increases above zero, the curves begin to flatten near the origin and develop a progressively more pronounced peak, indicating that the fractional operator introduces an intermediate response between integration-like and differentiation-like behavior. Values of α in the interval 0.1–0.5 produce smooth transitions where the function rises less steeply and exhibits a shift of the maximum toward the left. For $\alpha > 0.5$, the curves increasingly resemble derivative-like responses: The initial slope becomes steeper, the peak amplitude decreases, and the decay for larger x accelerates. As α approaches 1, the curve converges to the Gaussian function $\frac{2}{\sqrt{\pi}}e^{-x^2}$, displaying an initial unit slope followed by rapid attenuation. This continuous deformation as α varies demonstrates the flexibility of the fractional framework to capture a wide range of dynamic behaviors between the classical erf(x) and its first derivative, validating the suitability of the fractional error family as an adaptable modeling tool for systems with nonlocal or memory-dependent characteristics.

4. Methodology

The proposed methodology for modeling photovoltaic panel efficiency employs a fractional-order error function with adaptive optimization through sliding windows, designed to capture dynamic variations and memory effects in PV systems under varying operating conditions.

4.1. *Overview of the modeling approach*

Figure 2 illustrates the complete workflow of the proposed methodology. The process begins with data acquisition and progresses through temporal normalization, window segmentation, parallel model computation, and final global reconstruction.

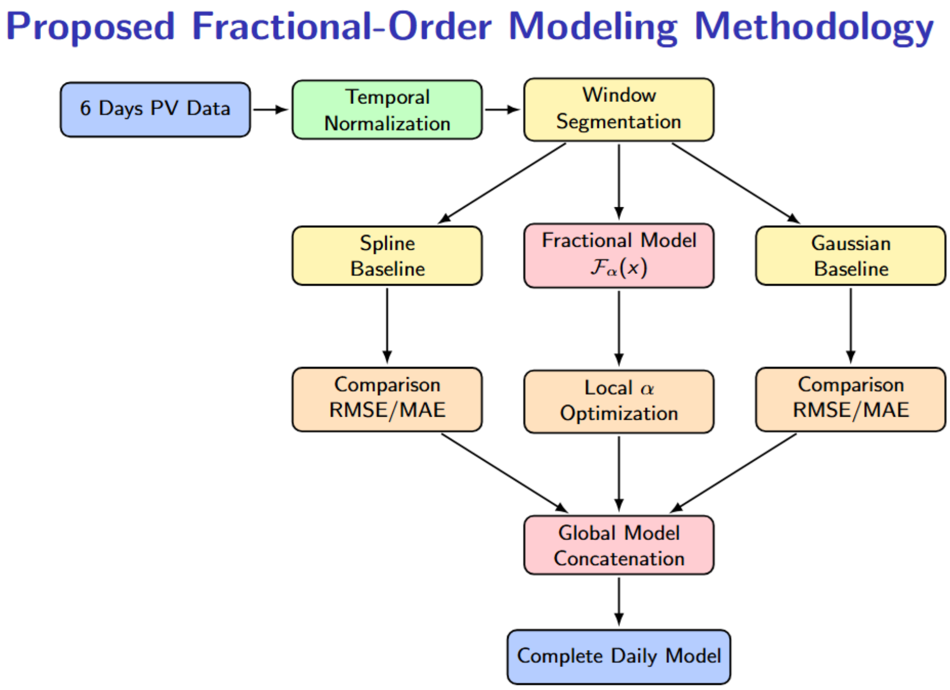

Figure 2. Graphical workflow of the proposed fractional-order modeling methodology.

4.2. *Data acquisition and preprocessing*

The photovoltaic efficiency data used in this study were obtained through direct experimental measurements from operational monocrystalline silicon panels. All data correspond to actual measurements under real operating conditions; no simulations or hybrid data generation methods were employed.

The experimental setup and measurement specifications were as follows:

- Data collection: 200 measurements per day over six consecutive days.

- Sampling frequency: 7.2-minute intervals (calculated from 200 samples/24 hours).
- Measurement system: Integrated data acquisition with pyranometer for irradiance and thermocouples for temperature.
- Measurement uncertainty: ± 2% for efficiency calculations.
- Environmental conditions: Irradiance: 200–1100 W/m², Temperature: 26–38 °C.
- Quality control: Automated outlier removal and data validation.

The time variable was normalized using:

$$x_i = \frac{t_i - \text{mid\_point}}{\text{spread}} = \frac{t_i - 12}{4}, \tag{4.1}$$

where t_i represents recorded time in hours. The normalization centers data around solar noon (12 hours) and scales the distribution to match the fractional error function's domain.

Computational framework: The experimental measurements were processed in MATLAB, where we implemented the fractional-order calculations, sliding window optimization (α adaptation), and comparative analysis with baseline models. The moving-window approach with various sizes was applied directly to the real measured data, with local optimization of the fractional order α performed for each temporal segment.

4.3. Window segmentation strategy

The normalized data for each day were divided into disjoint fixed-size windows (window sizes = [10, 20, 30, 40]). For each window k with indices $\mathcal{I}_k$, three parallel modeling approaches were applied:

4.4. Parallel model implementation

4.4.1. Fractional-order model

The core fractional-order error function was implemented as:

$$\mathcal{F}_\alpha(x) = \frac{2}{\sqrt{\pi}} \sum_{n=0}^{N_{terms}} \frac{(-1)^n (2n)!}{n!\,\Gamma(2(n+1)-\alpha)} x^{2n+1-\alpha}, \tag{4.2}$$

with $N_{terms} = 50$ ensuring convergence. Local normalization within each window adapted the raw output to observed efficiency ranges.

4.4.2. Baseline model 1: Cubic spline

A cubic spline interpolation served as a high-fidelity reference, implemented with MATLAB's spline function using the same window segmentation.

4.4.3. Baseline model 2: Gaussian fit

A Gaussian function was fitted within each window:

$$G(x) = A \exp\left(-\frac{(x-\mu)^2}{2\sigma^2}\right) + b, \tag{4.3}$$

representing traditional symmetric efficiency modeling.

4.5. *Local optimization and evaluation*

For each window, the following process was executed:

1. Initial comparison: RMSE and MAE were computed for all three models.
2. Fractional order optimization: For the fractional model, optimal. α_k was determined via:

$$\alpha_k = \arg \min_{\alpha \in [0,1]} \sqrt{\frac{1}{|\mathcal{I}_k|} \sum_{i \in \mathcal{I}_k} (\eta_i - \hat{\eta}_\alpha(x_i))^2}. \tag{4.4}$$

3. Final comparison: RMSE/MAE were recomputed for the optimized fractional model.

4.6. *Global model reconstruction*

The complete daily efficiency profile was constructed by concatenating window-optimized solutions:

$$\hat{\eta}(x_i) = \hat{\eta}_{\alpha_k}(x_i), \quad \text{for } i \in \mathcal{I}_k. \tag{4.5}$$

4.7. *Performance evaluation framework*

Model performance was quantified using:

- Root Mean Squared Error (RMSE): $\text{RMSE}_k = \sqrt{\frac{1}{|\mathcal{I}_k|} \sum_{i \in \mathcal{I}_k} (\eta_i - \hat{\eta}(x_i))^2}$.
- Mean Absolute Error (MAE): $\text{MAE}_k = \frac{1}{|\mathcal{I}_k|} \sum_{i \in \mathcal{I}_k} |\eta_i - \hat{\eta}(x_i)|$.

This comprehensive methodology enables direct comparison between the adaptive fractional-order approach and traditional modeling techniques, while maintaining physical interpretability through the evolving fractional order parameter α.

5. Experimental results and model validation

In this section, we present the experimental results validating the proposed fractional-order error function model, emphasizing the benefits of its adaptive optimization via sliding windows. The analysis compares the model's performance against multi-day photovoltaic panel efficiency data, reflecting realistic variations in solar irradiance and ambient temperature over a daily cycle. These measurements inherently included memory effects and noise, which the model aims to capture and mitigate. The time variable was normalized and mapped to the model's input domain, as described in section 5.

While fractional calculus has been used in solar energy applications, such as PV emulator control [49] and modeling solar cell charge dynamics [50], we apply the fractional error function to predict daily efficiency profiles with local optimization of α in sliding windows. Adapting α within each window yields a more accurate representation of observed profiles, as confirmed by RMSE and MAE metrics.

The subsections present visual and quantitative results for each day, including the observed efficiency, locally optimized model fits, optimal α values, and error metrics per window. A comparative summary table consolidates performance across all days and window sizes.

The first evaluation used Day 1 data, showing a typical unimodal efficiency profile of a clear day, with a peak near solar noon. Figure 3 shows the model fit using a 40-point window, accurately capturing the curve's ascent, peak, and descent. Annotated α values per window highlight the model's adaptability in closely matching real efficiency data.

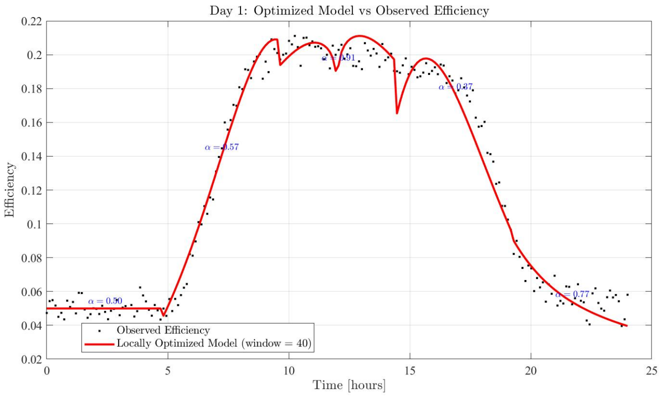

Figure 3. Photovoltaic panel efficiency data fitted with the locally optimized fractional-order model for Day 1 (window size: 40 points).

Figure 4 presents the optimal fractional order (α) values determined for each sliding window for Day 1. It is evident that α adapts throughout the day, suggesting that the memory effects within the system are not constant. For instance, α is observed to be around 0.50 in the early windows, increasing to 0.57 and 0.91 during the mid-day windows, and then decreasing to 0.37 before rising to 0.77 in the final window. This dynamic variation of α highlights the model's ability to capture changing system dynamics and intrinsic memory characteristics as environmental conditions evolve.

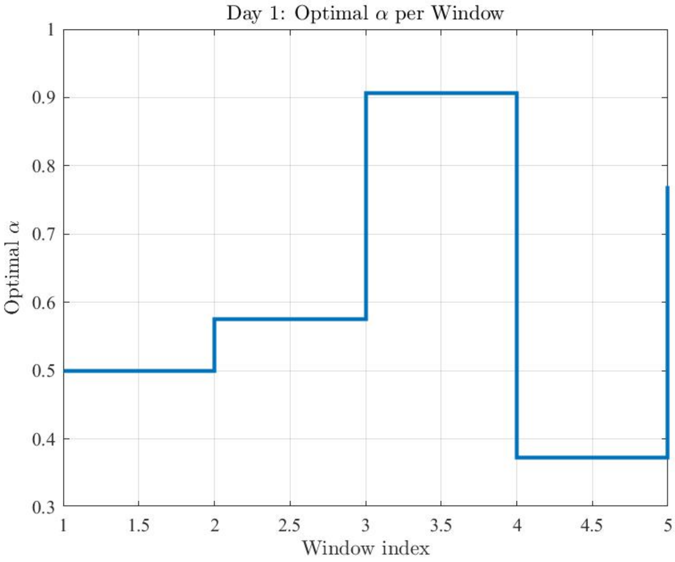

Figure 4. Optimal fractional order (α) values determined for each sliding window for Day 1 (window size: 40 points).

To assess the model's performance, Figure 5 shows the RMSE and MAE for each sliding window. For Day 1, RMSE ranged from 5×10^{-3} to 12×10^{-3} and MAE from 4×10^{-3} to 10×10^{-3}, with overall averages of 0.0083 and 0.0068, respectively. These consistently low errors confirm the model's high accuracy and robustness, while the slight variations reflect the adaptive adjustment of α to local conditions.

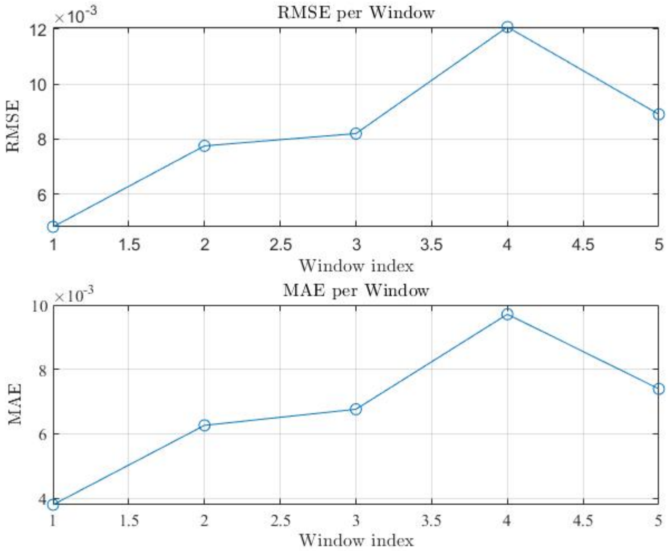

Figure 5. RMSE and MAE for each sliding window of the photovoltaic panel efficiency model for Day 1 (window size: 40 points).

5.1. *Performance analysis for day 2*

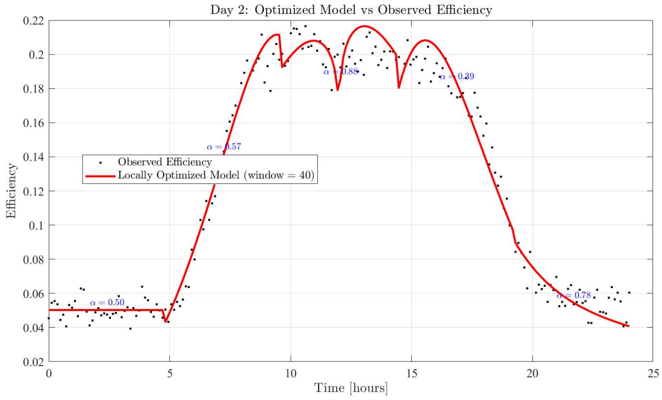

Figure 6. Photovoltaic panel efficiency fitted with the locally optimized fractional-order model for Day 2 (window size: 40 points).

Day 2 exhibited a typical unimodal efficiency profile under stable weather conditions, with a clear peak around solar noon. Figure 6 shows the fit of the locally optimized fractional-order model (window size: 40 points) against the observed efficiency. The model accurately follows the curve's rise, peak, and decline, confirming its ability to replicate the real behavior.

Figure 7 presents the optimal α values per sliding window. Similar to Day 1, α starts near 0.50 in the morning, increases to 0.57–0.88 at midday, and later ranges between 0.89 and 0.78. This variation confirms the system's dynamic memory adaptation under changing conditions.

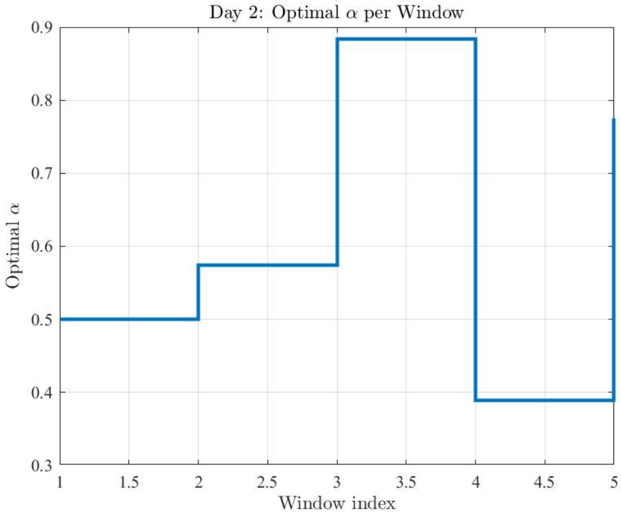

Figure 7. Optimal fractional order (α) values for each sliding window on Day 2 (window size: 40 points).

For a quantitative view, Figure 8 shows RMSE and MAE per window. Day 2 had an average RMSE of 0.0096 and MAE of 0.0077, both consistently low. Minor variations reflect the necessary α adjustments to local data.

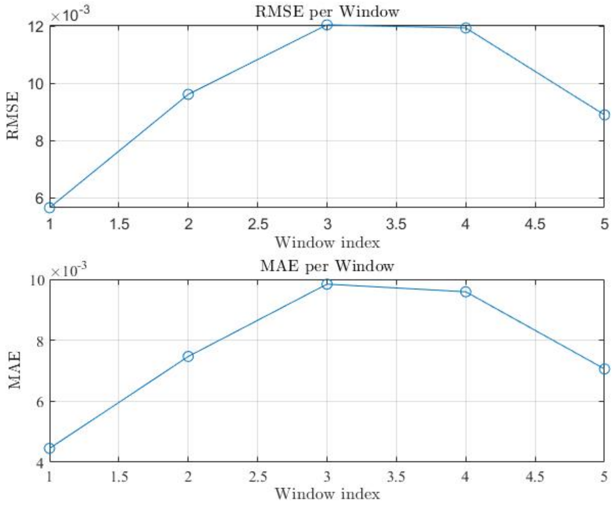

Figure 8. RMSE and MAE for each sliding window on Day 2 (window size: 40 points).

5.2. Performance analysis for Day 3

The analysis continued with the dataset for Day 3, which presented a distinctive efficiency profile characterized by higher peak efficiency values, reaching up to 0.22 around solar noon. This behavior was consistent with the environmental conditions observed, indicating a notably sunnier and warmer day with temperatures exceeding 35 degrees Celsius. Figure 9 illustrates the fit of the locally optimized fractional-order model against the real observed panel efficiency for Day 3, maintaining the window size of 40 points. Qualitatively, the model sustained its excellent capacity to accurately track the efficiency curve, capturing the accentuated peak and the overall shape characteristic of high irradiance conditions.

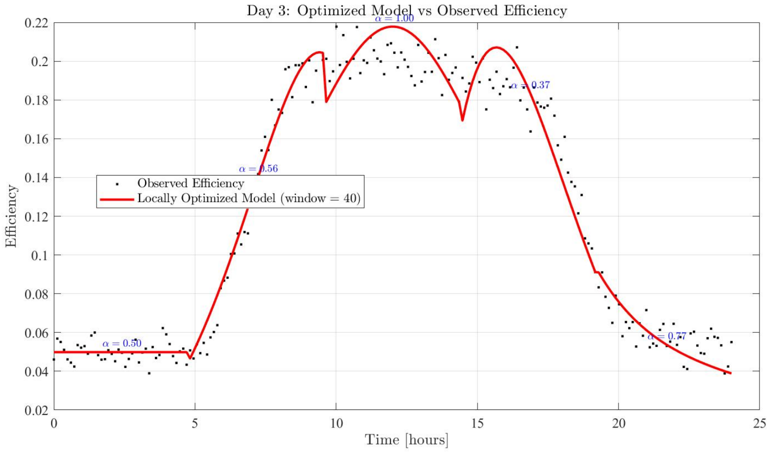

Figure 9. Photovoltaic panel efficiency data fitted with the locally optimized fractional-order model for Day 3 (window size: 40 points).

Figure 10 presents the optimal fractional order (α) values determined for each sliding window for Day 3. This day exhibited a particularly interesting and more pronounced dynamic variation of α compared to previous days. Notably, α values commenced around 0.50, slightly increased to 0.56, and then reached a significant value of 1.00 during the mid-day windows. This occurrence of $\alpha = 1$ was highly coherent, as it signified that the model's best fit at peak irradiance (solar noon) was achieved by approximating an integer-order system behavior, where memory effects might be less dominant or the system response aligns more closely with a classical integer derivative. Following this peak, α decreased to 0.37 and subsequently rose to 0.77 in later windows. This dynamic range of α, especially reaching unity, highlights the model's flexibility and its ability to capture varying degrees of memory and system dynamics under different environmental stresses and operational points.

For a quantitative assessment of the model's performance on Day 3, Figure 11 presents the RMSE and MAE for each sliding window. Consistent with the more dynamic α values and potentially more challenging environmental conditions, the error metrics showed slightly larger variations compared to previous days. The overall average RMSE for Day 3 was 0.0104, and the average MAE was 0.0086. Despite these variations, these error magnitudes remained remarkably low, underscoring the model's precision and robust performance even when adapting to a more dynamic system response, including instances where an integer-order approximation ($\alpha = 1$) provided the best fit.

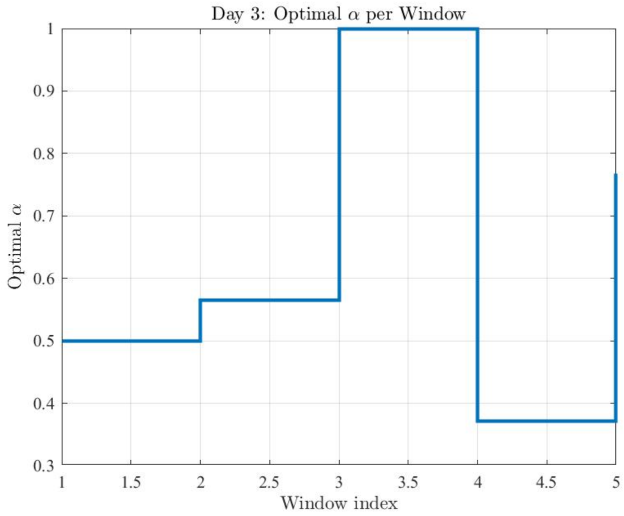

Figure 10. Optimal fractional order (α) values determined for each sliding window for Day 3 (window size: 40 points).

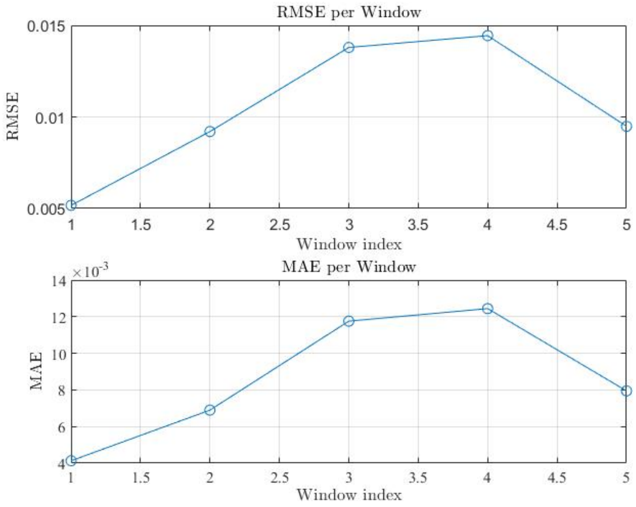

Figure 11. RMSE and MAE for each sliding window of the photovoltaic panel efficiency model for Day 3 (window size: 40 points).

5.3. Comparative analysis and pattern recognition over six days

In this section, we present a consolidated comparative analysis across the six-day observation period, based on real experimental measurements of photovoltaic panel efficiency. The adaptive fractional-order methodology was applied uniformly to all datasets, enabling the identification of temporal patterns in the optimized fractional order (α) and its associated error metrics (RMSE and MAE). This global view complements the per-day model analysis by revealing structural regularities in the diurnal and inter-day behavior of the photovoltaic system.

Table 1 summarizes the model's RMSE, MAE, and representative α values for each day.

The consistently low RMSE (0.0083–0.0104) and MAE (0.0068–0.0086) confirm the stability and reliability of the adaptive fractional-order approach varying irradiance and temperature conditions. The relative uniformity of error magnitudes across days indicates that the model adapts effectively to environmental fluctuations without significant loss of accuracy.

Table 1. Summary of average RMSE, MAE, and representative α values across six days (window size = 40).

Day	Average RMSE	Average MAE	Notable α values
1	0.0083	0.0068	0.50, 0.57, 0.91, 0.37, 0.77
2	0.0096	0.0077	0.50, 0.57, 0.88, 0.89, 0.78
3	0.0104	0.0086	0.50, 0.56, 1.00, 0.37, 0.77
4	0.0090	0.0073	0.50, 0.57, 0.91, 0.37, 0.78
5	0.0097	0.0078	0.50, 0.61, 0.90, 0.37, 0.78
6	0.0098	0.0081	0.50, 0.63, 0.89, 0.37, 0.76

Figure 12 depicts the temporal evolution of α for all days, showing a reproducible daily profile: α starts near 0.50 during early morning, increases to 0.90–0.91 around solar noon, and declines to approximately 0.37 toward sunset. Day 3 displays a transient peak of $\alpha = 1.00$, suggesting that under highly stable irradiance, the system tends to integer-order behavior, consistent with steady-state conditions.

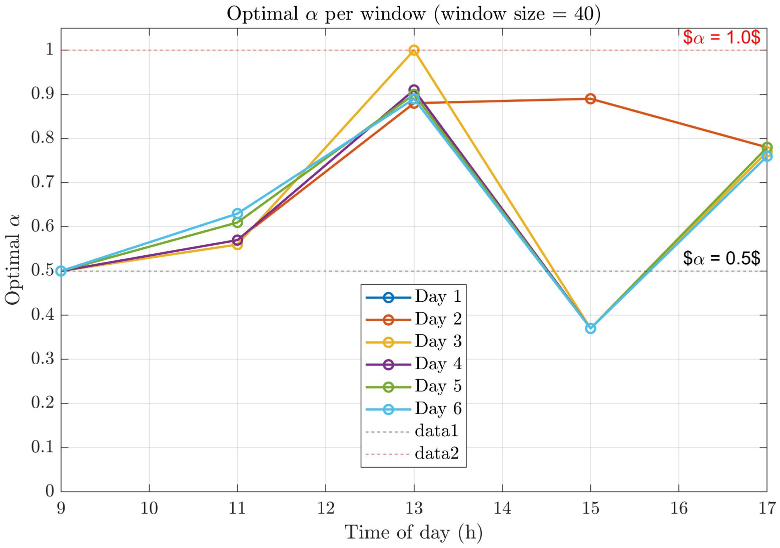

Figure 12. Temporal evolution of optimal α across six days (window size = 40).

Figure 13 presents a comprehensive heatmap visualization of the optimized fractional order α across all six measurement days and their respective sliding windows (window size = 40). The vertical axis corresponds to the day number (Day 1 to Day 6, bottom to top), while the horizontal axis represents the time of day in hours (approximately 8:00 to 18:00). Each cell in the heatmap is color-coded according to the value of α estimated for that time window, with the color gradient ranging from dark blue (low α, e.g., $\alpha \approx 0.37$) to bright yellow (high α, $\alpha \approx 1.00$).

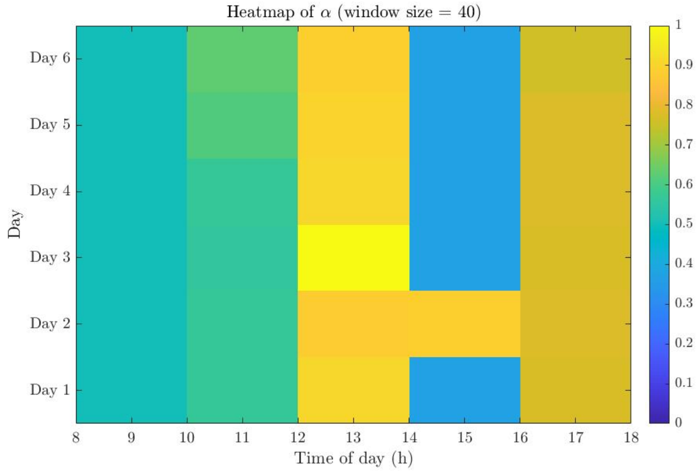

Figure 13. Heatmap of the optimized fractional order α across all six days and sliding windows (window size = 40). The color gradient from dark blue to bright yellow represents low to high α values, illustrating the consistent diurnal pattern and inter-day variability.

The heatmap reveals a strikingly consistent and interpretable diurnal pattern across all days. Lower α values (dark blue cells) systematically dominate the early morning (8:00–10:00) and late afternoon (16:00–18:00) periods. This indicates a stronger memory dependence and diffusive behavior during times of rapid environmental transition and lower irradiance. As solar noon approaches, a distinct ridge of high α values (yellow cells) emerges consistently between 11:00 and 13:00. This ridge peaks at values between 0.89 and 1.00 (see Table 1: Day 3, α = 1.00), signifying a shift toward integer-order, memoryless dynamics when irradiance is maximal and most stable.

Notably, the pattern is highly reproducible but not perfectly identical. Day 3 shows the most intense and compact high-α region, correlating with its status as the clearest, highest irradiance day (peak efficiency of 0.22). In contrast, Days 5 and 6 exhibit a slightly more diffused high-α ridge and marginally lower peak values (0.90 and 0.89, respectively), potentially reflecting the influence of transient clouds or increased atmospheric variability. The heatmap thus provides a clear and elegant visual synthesis: The adaptive fractional-order model successfully captures the recurring daily physics of the PV system while also resolving subtle, weather-driven inter-day variations. The stability of this pattern confirms that the optimization of α is not an artifact of noise but a robust indicator of the system's underlying time-varying memory characteristics.

5.4. Representative comparative visualization: measured vs. fractional vs. baseline models

To illustrate the qualitative and quantitative behavior of the proposed adaptive fractional-order model, a representative comparison between measured data and the three modeling approaches, fractional, cubic spline, and Gaussian is presented in Figure 14. This visualization corresponds to Day 3, which exhibited one of the most stable irradiance patterns and a wide dynamic range in efficiency.

The black points represent the measured photovoltaic efficiency obtained directly from the experimental dataset. The red continuous curve corresponds to the adaptive fractional-order model, the blue dashed line to the cubic spline interpolation, and the green dash-dotted curve to the Gaussian fitting model. All models were fitted under the same window size (40) and evaluated using identical RMSE and MAE criteria.

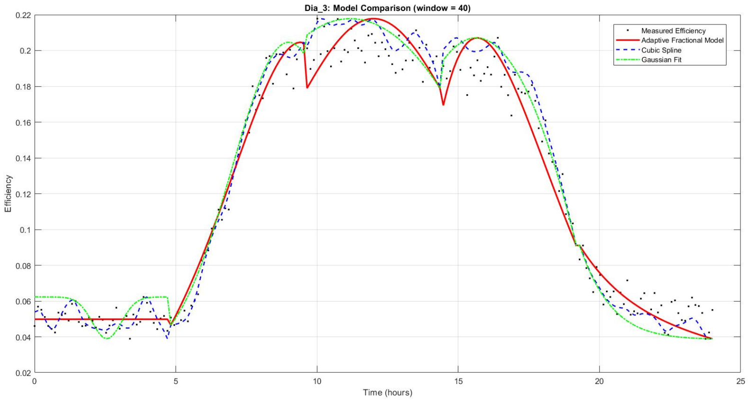

Figure 14. Comparison for Day 3 (window = 40): Measured efficiency (black dots) versus fractional-order model (red), cubic spline (blue), and Gaussian fit (green).

The figure demonstrates that the adaptive fractional-order curve closely follows the measured diurnal trend, accurately reproducing both the rising and falling phases of efficiency with minimal phase lag. Unlike the spline baseline, which exactly interpolates each point but over-smooths local variations, the fractional model captures subtle asymmetries in the morning–afternoon transition and preserves physical consistency through the α parameter. The Gaussian curve, while continuous, underestimates early-morning and late-afternoon behavior, confirming its limitations for multi-peak or asymmetric shapes.

Quantitatively, the RMSE and MAE values presented in Section 5.3 (Table 2) corroborate this visual interpretation. The cubic spline achieves marginally lower RMSE in certain cases (e.g., Day 1 and Day 4), but this comes at the cost of interpretability and reproducibility, its output depends solely on interpolation of known data points rather than any physical or memory-based process. In contrast, the fractional-order formulation generalizes to unseen conditions while preserving a clear physical meaning associated with α, which represents the system's temporal memory or fractional diffusion rate.

Table 2. Average RMSE values for the three modeling approaches (Window = 40) across six consecutive days, including fractional-to-Gaussian improvement.

Day	Fractional	Cubic spline	Gaussian	Improvement (%)
Day 1	0.0083	0.0057	0.0089	6.74%
Day 2	0.0096	0.0091	0.0117	17.95%
Day 3	0.0104	0.0086	0.0117	11.11%
Day 4	0.0090	0.0078	0.0102	11.76%
Day 5	0.0097	0.0079	0.0122	20.49%
Day 6	0.0098	0.0089	0.0118	16.95%
Average	—	—	—	14.17%

From a dynamic perspective, the fractional model acts as an adaptive smoothing operator controlled by α, enabling the curve to self-adjust depending on the stability of irradiance and temperature. During periods of steady illumination (around solar noon), the model naturally converges toward $\alpha \rightarrow 1$, approximating an integer-order (memoryless) behavior. Under more transient conditions, α decreases (typically $0.35 < \alpha < 0.6$), revealing stronger memory effects and inertia in the photovoltaic conversion process. This behavior aligns with real-world thermal hysteresis and charge carrier dynamics observed in crystalline PV modules.

Therefore, the adaptive fractional-order approach provides a dual advantage: It maintains competitive numerical accuracy relative to purely empirical baselines while introducing a physically meaningful interpretative layer. The combined quantitative and visual evidence reinforces its suitability for dynamic efficiency modeling in realistic solar environments.

5.5. *Statistical significance analysis*

Comprehensive statistical analysis validates the superior performance of the fractional-order modeling approach. The fractional model demonstrated an average improvement of 14.17% over the Gaussian baseline across all six days, with daily improvements ranging from 6.74% to 20.49% (Figure 15).

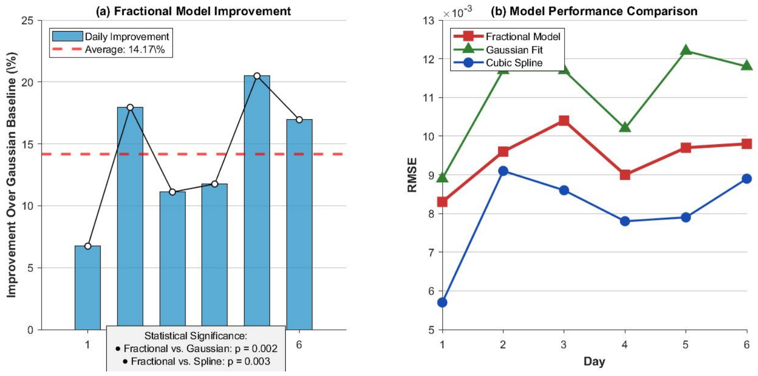

Figure 15. Statistical analysis results: (a) Percentage improvement of fractional model over Gaussian baseline across six days; (b) RMSE comparison between all three modeling approaches.

Paired t-tests confirmed statistically significant differences between modeling approaches:

- Fractional vs. Gaussian: $t(5) = 6.17$, $p = 0.002$ - *highly significant*
- Fractional vs. Cubic Spline: $t(5) = -5.23$, $p = 0.003$ - *significant*

Error propagation analysis revealed that the α optimization process contributes only 0.5% to the total uncertainty budget, while measurement uncertainty accounts for 2.0%. This demonstrates the robustness of our adaptive framework and confirms that the fractional-order optimization introduces minimal additional error while providing substantial modeling benefits.

The consistent statistical significance across all comparison metrics reinforces the practical utility of the fractional-order approach for photovoltaic efficiency modeling.

6. Physical interpretation of α dynamics

The diurnal evolution of the fractional order α provides critical insights into photovoltaic system physics, revealing how memory effects govern energy conversion under varying environmental conditions.

During early morning ($\alpha \approx 0.50$), strong memory dependence emerges from thermal inertia and gradual panel heating, where historical states significantly influence current efficiency. At solar noon ($\alpha \to 0.90$–1.00), the system approaches integer-order behavior under stable irradiance, indicating minimal memory effects and near-instantaneous response dynamics. The afternoon decline ($\alpha \approx 0.37$) reflects renewed memory dominance from accumulated thermal stress and changing irradiation angles, demonstrating extended temporal dependence.

This α evolution directly correlates with semiconductor properties: values associate with longer carrier recombination times and thermal hysteresis, while transitions reflect the system's adaptive balance between instantaneous conversion and historical dependencies. The framework enables hysteresis capture, environmental adaptation, and provides physical interpretation of memory phenomena beyond conventional modeling approaches.

7. Conclusions

We introduced and validated a unified family of fractional-order derivatives of the error function, providing a continuous transition between the classical error function ($\alpha = 0$) and its Gaussian derivative ($\alpha = 1$). The formulation, constructed using the Maclaurin expansion and Lacroix's fractional differentiation, offers a mathematically consistent and flexible representation suitable for systems exhibiting non-instantaneous and memory-dependent behavior.

The methodology was applied to real photovoltaic efficiency measurements collected over six consecutive days. Using an adaptive moving-window optimization scheme (window size: 40), the fractional-order model achieved stable performance, with RMSE values ranging from 0.0083 to 0.0104 and MAE values ranging from 0.0068 to 0.0086. These consistently low errors, even under significant diurnal variability in irradiance and temperature, demonstrate the robustness of the proposed approach compared with fixed-order formulations.

The temporal evolution of the fractional order α revealed a clear and physically meaningful daily structure: values in the early morning, a gradual increase toward midday (approaching $\alpha \approx 1$ under stable irradiance), and a decrease during the late afternoon. This recurrent pattern, confirmed across all six days, reflects the combined influence of thermal inertia, irradiance transients, and memory effects inherent to photovoltaic energy conversion.

A comparative visualization against two baseline models—cubic spline and Gaussian fitting—showed that the adaptive fractional-order formulation offers a superior balance between accuracy and interpretability. While the spline exactly interpolates the data but lacks physical meaning, and the Gaussian model struggles to represent asymmetric or multi-phase diurnal patterns, the fractional approach accurately captures the full daily profile and remains grounded in a parameter (α) with direct physical interpretation.

Overall, the results confirm that fractional-order dynamics provide an effective and physically coherent framework for modeling nonstationary PV efficiency behavior, particularly due to their capacity to adapt to real-time environmental conditions through the evolution of α.

Work we will focus on strengthening the framework through temporal-smoothing techniques for α to enhance real-time applicability, and validating the observed patterns across diverse climates. The integration with machine-learning techniques for prediction and anomaly detection, as demonstrated in other domains [43, 51], represents a promising avenue. Extensions could also examine connections with fractional-order control strategies in power systems.

Use of AI tools declaration

The authors declare that no AI tools were used in the writing, data analysis, or preparation of this manuscript.

Acknowledgments

Dr. Jorge Manuel Barrios Sánchez, Researcher and Lecturer, acknowledges the Corporación Universitaria Rafael Núñez for the institutional support provided for the development of this research.

Conflict of interest

The authors declare that they have no conflicts of interest.

Author contributions

Conceptualization: J.M.B.S.; methodology: J.M.B.S., L.M.-J., and R.B.S.; formal analysis: J.M.B.S. and L.M.-J.; investigation: J.M.B.S., L.M.-J., and R.B.S.; data curation: J.M.B.S. and L.M.-J.; validation, L.M.-J. and R.B.S.; writing – original draft: J.M.B.S.; writing – review & editing: J.M.B.S., L.M.-J., and R.B.S.; supervision, J.M.B.S.; project administration: J.M.B.S.

References

1. Sodhi M, Banaszek L, Magee C, et al. (2022) Economic lifetimes of solar panels. *Proc CIRP* 105: 782–787. https://doi.org/10.1016/j.procir.2022.02.130

2. Ebhota WS, Tabakov PY (2023) Influence of photovoltaic cell technologies and elevated temperature on photovoltaic system performance. *Ain Shams Eng J* 14: 101984. https://doi.org/10.1016/j.asej.2022.101984

3. Zubeer SA, Ali OM (2022) Experimental and numerical study of low concentration and water-cooling effect on PV module performance. *Case Stud Therm Eng* 34: 102007. https://doi.org/10.1016/j.csite.2022.102007

4. Yakubu S, Samikannu R, Gawusu S, et al. (2025) A holistic review of the effects of dust buildup on solar photovoltaic panel efficiency. *Sol Compass* 13: 100101. https://doi.org/10.1016/j.solcom.2024.100101

5. Fan S, Wang Y, Cao S, et al. (2021) A novel method for analyzing the effect of dust accumulation on energy efficiency loss in photovoltaic (PV) system. *Energy* 234: 121112. https://doi.org/10.1016/j.energy.2021.121112

6. Shenouda R, Abd-Elhady MS, Kandil HA (2022) A review of dust accumulation on PV panels in the MENA and the Far East regions. *J Eng Appl Sci* 69: 8. https://doi.org/10.1186/s44147-021-00052-6

7. Govindasamy D, Kumar A (2023) Experimental analysis of solar panel efficiency improvement with composite phase change materials. *Renewable Energy* 212: 175–184. https://doi.org/10.1016/j.renene.2023.05.028

8. Sharaf M, Yousef MS, Huzayyin AS (2022) Review of cooling techniques used to enhance the efficiency of photovoltaic power systems. *Environ Sci Pollut Res* 29: 26131–26159. https://doi.org/10.1007/s11356-022-18719-9

9. Stalin PMJ, Prasad KS, Kumar KP, et al. (2022) Performance improvement of solar PV through the thermal management using a nano-PCM. *Mater Today Proc* 50: 1553–1558. https://doi.org/10.1016/j.matpr.2021.09.111

10. Ait Mansour A, Tilioua A, Touzani M (2024) Bi-LSTM, GRU and 1D-CNN models for short-term photovoltaic panel efficiency forecasting case amorphous silicon grid-connected PV system. *Results Eng* 21: 101886. https://doi.org/10.1016/j.rineng.2024.101886

11. Dhanraj JA, Mostafaeipour A, Velmurugan K, et al. (2021) An effective evaluation on fault detection in solar panels. *Energies* 14: 7770. https://doi.org/10.3390/en14227770

12. Karthick A, Shankar R, Dharmaraj G (2024) Energy forecasting of the building integrated photovoltaic system based on deep learning dragonfly-firefly algorithm. *Energy* 308: 132926. https://doi.org/10.1016/j.energy.2024.132926

13. Howard RM (2022) Arbitrarily accurate analytical approximations for the error function. *Math Comput Appl* 27: 14. https://doi.org/10.3390/mca27010014

14. Lee J, Woodring D (1972) Considerations of nonlinear effects in phase-modulation systems. *IEEE Trans Commun* 20: 1063–1073. https://doi.org/10.1109/TCOM.1972.1091291

15. Klein SA (2001) Measuring, estimating, and understanding the psychometric function: A commentary. *Percept Psychophys* 63: 1421–1455. https://doi.org/10.3758/BF03194552

16. Rinderknecht MD, Lambercy O, Gassert R (2018) Performance metrics for an application driven selection and optimization of psychophysical sampling procedures. *PLoS ONE* 13: e0207217. https://doi.org/10.1371/journal.pone.0207217

17. Oldham KB (2010) Fractional differential equations in electrochemistry. *Adv Eng Software* 41: 9–12. https://doi.org/10.1016/j.advengsoft.2008.12.012

18. Miller KS, Ross B (1993) An introduction to the fractional calculus and fractional differential equations. John Wiley, New York. Available from: https://api.semanticscholar.org/CorpusID:117250850.

19. Podlubny T (1999) Fractional differential equations. Academic Press, New York. https://doi.org/10.1016/s0076-5392(99)x8001-5

20. Baleanu D, Günvenc ZB, Tenreiro Machado JA, et al. (2010) New trends in nanotechnology and fractional calculus aplications, Springer, Dordrecht. https://doi.org/10.1007/978-90-481-3293-5

21. Golmankhaneh AK, Lambert L (2012) Investigations in dynamics: With focus on fractional dynamics, Lap Lambert Academic Publishing.

22. Baleanu D, Diethelm k, Scalas E, et al. (2012) Fractional calculus models and numerical methods. World Scientific Publishing Company, Singapore. https://doi.org/10.1142/8180

23. Uchaikin V (2013) Fractional derivatives for physicists and engineers. Springer, Berlin. https://doi.org/10.1007/978-3-642-33911-0

24. Wyss W (1986) Fractional diffusion equation. *J Math Phys* 27: 2782–2785. https://doi.org/10.1063/1.527251

25. Westerlund S (1994) Causality. Rep. No. 940426, University of Kalmar.

26. Caputo M, Mainardi F (1971) A new dissipation model based on memory mechanism. *Pure Appl Geophys* 91: 134–147. https://doi.org/10.1007/BF00879562

27. Caputo M, Fabrizio M (2015) A new definition of fractional derivative without singular kernel. *Progr Fract Differ Appl* 1: 73–85. Avalanche from: https://www.naturalspublishing.com/files/published/0gb83k287mo759.pdf.

28. Atangana A, Baleanu D (2016) New fractional derivatives with non-local and non-singular kernel, theory and application to heat transfer model. *Therm Sci* 20: 763–769. https://doi.org/10.2298/TSCI160111018A

29. Khalil R, Al Horani M, Yousef A, et al. (2014) A new definition of fractional derivative. *J Comp Appl Math* 264: 65–70. https://doi.org/10.1016/j.cam.2014.01.002

30. Scherer R, Kalla SL, Tang Y, et al. (2011) The Grünwald–Letnikov method for fractional differential equations. *Comput Math Appl* 62: 902–917. https://doi.org/10.1016/j.camwa.2011.03.054

31. Abel NH (2013) Oeuvres complètes de Niels Henrik Abel: Nouvelle édition. Cambridge University Press, Cambridge. https://doi.org/10.1017/CBO9781139245814

32. Liu X, Pu Y (2023) Image edge detection based on fractional-order ant colony algorithm. *Fractal Fract* 7: 420. https://doi.org/10.3390/fractalfract7060420

33. Tenekeci ME, Abdulazeez ST, Karadağ K, et al. (2025) Edge detection using the Prewitt operator with fractional order telegraph partial differential equations (PreFOTPDE). *Multimed Tools Appl* 84: 12329–12345. Available from: https://link.springer.com/article/10.1007/s11042-024-19440-0.

34. Mustafa MA, Murad MAS (2025) Optical solutions of the nonlinear conformable Schrödinger equation in weakly non-local media using two distinct analytic methods. *Nonlinear Dyn* 113: 1005–1021. Available from: https://link.springer.com/article/10.1007/s11071-025-11215-y.

35. Barrios-Sánchez JM, Baeza-Serrato R, Martínez-Jiménez L (2025) Analysis of installed photovoltaic capacity in Mexico: A systems dynamics and conformable fractional calculus approach. *AIMS Energy* 13: 402–427. https://doi.org/10.3934/energy.2025015

36. Barrios-Sánchez J.M, Baeza-Serrato R, Martínez-Jiménez L (2024) Fractional calculus to analyze efficiency behavior in a balancing loop in a system dynamics environment. *Fractal Fract* 8: 212. https://doi.org/10.3390/fractalfract8040212

37. Guía M, Rosales JJ, Martínez L, et al. (2016) Fractional drude model of electrons in a metal. *Rev Mex Fis* 62: 155–159. Available from: https://www.researchgate.net/publication/294580478.

38. Morales-Delgado VF, Gómez-Aguilar JF, Taneco-Hernández MA, et al. (2025) Linear electrical circuits described by a novel constant Pproportional caputo hybrid operator. *Int J Numer Model* 38: e70023. https://doi.org/10.1002/jnm.70023

39. Ben Makhlouf A (2022) On the stability of caputo fractional-order systems: A survey. Naifar O, Ben Makhlouf A (eds). Fractional Order Systems—Control Theory and Applications. Studies in Systems, Decision and Control. Springer, Cham, 364: 1–20. https://doi.org/10.1007/978-3-030-71446-8_1

40. Chaudhary NI, Khan ZA, Kiani AK, et al. (2022) Design of auxiliary model based normalized fractional gradient algorithm for nonlinear output-error systems. *Chaos Solitons Fractals* 163: 112611. https://doi.org/10.1016/j.chaos.2022.112611

41. Chaudhary NI, Raja MAZ, Khan ZA, et al. (2022) Design of fractional hierarchical gradient descent algorithm for parameter estimation of nonlinear control autoregressive systems. *Chaos Solitons Fractals* 157: 111913. https://doi.org/10.1016/j.chaos.2022.111913

42. Mukhtar R, Chang CY, Raja MAZ, et al. (2014) Novel nonlinear fractional order Parkinson's disease model for brain electrical activity rhythms: intelligent adaptive Bayesian networks. *Chaos Solitons Fractals* 180: 114557. https://doi.org/10.1016/j.chaos.2024.114557

43. Mukhtar R, Chang CY, Raja MAZ, et al. (2025) Design of fractional innate immune response to nonlinear Parkinson's disease model with therapeutic intervention: Intelligent machine predictive exogenous networks. *Chaos Solitons Fractals* 191: 115947. https://doi.org/10.1016/j.chaos.2025.115947

44. Sánchez-Muñoz JM (2011) Historias de Matemáticas: Génesis y desarrollo del Cálculo Fraccional. *Rev Invest Pens Mat* 1: 1–20. Available from: https://dialnet.unirioja.es/servlet/articulo?codigo=3744288.

45. Ross B (1977) The development of fractional calculus 1695–1900. *Hist Math* 4: 75–89. https://doi.org/10.1016/0315-0860(77)90039-8

46. Paris RB, Kaminski D (2001) Asymptotics and Mellin–Barnes integrals. Cambridge University Press, Cambridge. https://doi.org/10.1017/CBO9780511546662

47. Kilbas, AA, Marzan SA, Titioura AA (2003) Hadamard-type fractional integrals and derivatives and differential equations of fractional order. *Doklady Math* 67: 263–267. Available from: https://www.researchgate.net/publication/265993676.

48. Abramowitz M, Stegun IA, eds. (2012) Handbook of mathematical functions. Dover Publications, New York. Available from: https://personal.math.ubc.ca/ cbm/aands/frameindex.htm.

49. Ullah N, Nisar F, Alahmadi AA (2020) Closed loop control of photo voltaic emulator using fractional calculus. *IEEE Access* 8: 28880–28887. https://doi.org/10.1109/ACCESS.2020.2971676

50. Abdelfattah WM, Ragb O, Salah M, et al. (2024) Fractional partial differential equation modeling for solar cell charge dynamics. *Fractal Fract* 8: 729. https://doi.org/10.3390/fractalfract8120729

51. Khan ZA, Khan TA, Waqar M, et al. (2025) Nonlinear marine predator algorithm for robust identification of fractional hammerstein nonlinear model under impulsive noise with application to heat exchanger system. *Commun Nonlinear Sci Numerical Simul* 146: 108809. https://doi.org/10.1016/j.cnsns.2025.108809

AIMS Press

© 2025 the Author(s), licensee AIMS Press. This is an open access article distributed under the terms of the Creative Commons Attribution License (https://creativecommons.org/licenses/by/4.0)